

PCCP

Accepted Manuscript



This is an *Accepted Manuscript*, which has been through the Royal Society of Chemistry peer review process and has been accepted for publication.

Accepted Manuscripts are published online shortly after acceptance, before technical editing, formatting and proof reading. Using this free service, authors can make their results available to the community, in citable form, before we publish the edited article. We will replace this *Accepted Manuscript* with the edited and formatted *Advance Article* as soon as it is available.

You can find more information about *Accepted Manuscripts* in the [Information for Authors](#).

Please note that technical editing may introduce minor changes to the text and/or graphics, which may alter content. The journal's standard [Terms & Conditions](#) and the [Ethical guidelines](#) still apply. In no event shall the Royal Society of Chemistry be held responsible for any errors or omissions in this *Accepted Manuscript* or any consequences arising from the use of any information it contains.

**Theoretical study on catalyzed selective photoreduction mechanism
for 4-bromobenzaldehyde in two different solvents**

Xiao Huang, Liang Peng*, Feng Long Gu*

Key Laboratory of Theoretical Chemistry of Environment, Ministry of
Education; School of Chemistry & Environment, South China Normal
University, Guangzhou, 510006, China. pengliang@m.scnu.edu.cn;

gu@scnu.edu.cn

Ruiqin Zhang

Department of Physics and Materials Science, City University of Hong Kong, Hong
Kong SAR, China.

Abstract Density functional theory (M06-2X) method have been employed to investigate the selective photoreduction mechanism in ethanol and acetonitrile solvents for 4-bromobenzaldehyde (4-BBA) reduced by photoelectron, which is produced by illumination of TiO₂. The solvent effect of ethanol and acetonitrile are considered by the SMD solvent model. The computational results show that the reaction is selective in different solvents. In ethanol solvent, the carbonyl reduction process is favored both in thermodynamics and kinetics, and 4-BBA could be reduced to the product of 4-bromobenzyl alcohol. However, owing to be not a good proton donor solvent, in acetonitrile, the debromination reduction process is favored. These results are in consistent with the experiment observation.

Keywords 4-BBA; Selective Reduction Mechanism; Photoelectron Reduction; DFT

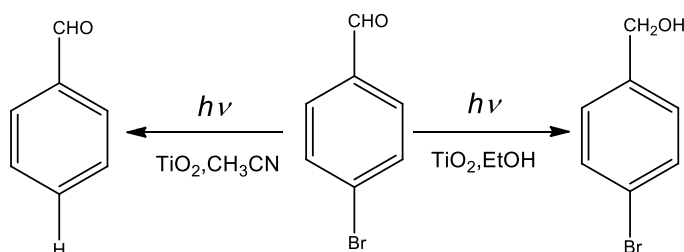
1 Introduction

The photocatalysis reaction on semiconductors has become an important research area, involving the converting solar energy^{1, 2}, purifying water and air, preventing metal corrosion, and so on. Owing to the ultraviolet-visible absorption³, high stability, non-toxicity, and the ability to be reused after recycles from the reaction medium⁴, TiO₂ has been the most widely used semiconductor.

In recent decades, more attention is paid in the photoelectron reduction of organic compounds on TiO₂, such as nitroarenes⁵⁻⁹, aldehydes^{3, 10}, ketones¹¹⁻¹⁵, and halogenated compounds¹⁶. In the case of photoreduction aldehydes, Yanagida et al.¹⁰ reported that the photoredox reaction of acetaldehyde and propionaldehyde in water, with ZnS as catalyst, observing reduction products ethanol, propanol and hydrogen.

Pruden et al.³ found that the aldehydes could be reduced to the corresponding alcohols using TiO_2 as photocatalyst, through two electrons transferring from the excited TiO_2 and followed by protonation. Moreover, the selective reduction of 4-BBA in 95% ethanol and in dry acetonitrile was investigated, in the study of which the reduction of carbonyl group occurs in ethanol while the debromination product benzaldehyde is obtained in dry acetonitrile, as shown in Scheme 1. Besides the photoelectron reduction, the alcohol radicals may be another reductive species. However, the roles of these radicals are still unclear^{17,18}. Ferry et al.¹⁷ pointed out that the alcohol radicals play no role in the observed reduction reaction for the nitro-compounds. But the other studies revealed that the alcohol radicals show strong reductive abilities¹⁹⁻²¹, thus these species could reduce 4-nitroaniline to *p*-phenylenediamine¹⁸.

Scheme 1 4-BBA being reduced into the two different reduction products in ethanol and acetonitrile solvents photo-catalyzed by TiO_2



However, only a few theoretical studies have been reported about the research of electron reduction mechanism, and these mainly focus on the catalyst surface reaction. Based on the first principles calculations, He et al.²² investigated the electron reduction of CO_2 on anatase (101) surfaces. They revealed that in photoreduction reaction of CO_2 , the anatase (101) surface played a pivotal role in facilitating electron and proton transfers. In addition, Lee et al.²³ employed the first principles calculations to study the electron reduction mechanisms of CO_2 on the surface of bulk anatase TiO_2 (101) and a small TiO_2 nanocluster, and the results indicated that the electron reduction process of converting CO_2 to CO was greatly promoted by the

presence of four-fold coordinated Ti atoms on the surface. Besides, Rotko et al.²⁴ investigated the reduction of polybrominated aromatics employing B3LYP method. They revealed that the polybrominated aromatics possess the low-lying $\sigma^*_{\text{C-Br}}$ orbitals, which play a key role in the reduction process.

To the best of our knowledge, it is unclear about the selective photoreduction mechanism in ethanol and acetonitrile solvents for 4-BBA catalyzed by TiO_2 . To fill the deficiency, we have been studied the electron reduction mechanism of organic compounds in solution²⁵. Specifically, on the basis of the experiment by Purden et al.³, we performed quantum chemical calculations to study the selective photoreduction mechanism of 4-BBA in ethanol and acetonitrile solvents.

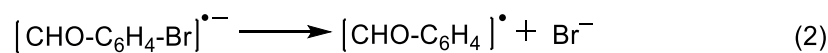
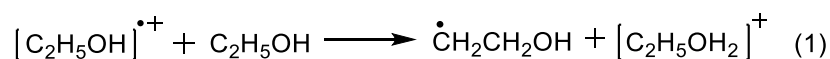
2 Computational details

All calculations were carried out employing Gaussian 09 program package²⁶. All structures of the reactants, intermediates, transition states, and corresponding products in the research system, were optimized using the M06-2X²⁷ functional with the 6-311G* basis set. For some of the reaction pathways, with the same basis set, B3LYP²⁸⁻³⁰ and MP2³¹⁻³⁵ methods were employed to make sure that the optimized structures of M06-2X are reliable. While single-point energy calculations based on MP2 optimized structures were done at the CCSD³⁶⁻³⁸/6-311G* level. The harmonic vibrational frequencies were calculated for all the optimized geometries at the same level to identify if the stationary points are minima (zero imaginary frequency) or transition states (only one imaginary frequency). The energies used in the research system were based upon the Gibbs free energies (the thermal correction included) calculated at a standard state of 298.15 K and 1 atm. An intrinsic reaction coordinate (IRC)³⁹ was used to calculate the reaction pathways to confirm each transition state

uniquely connecting the reactant to the product. Additionally, for all calculations mentioned above, to mimic experimental conditions, we took the solvent effects into account by using the SMD⁴⁰ solvation model, which is based on a self-consistent reaction field treatment of bulk electrostatics that involves an integration of the nonhomogeneous Poisson equation in terms of the integral-equation-formalism polarizable continuum model (IEF-PCM), and on a cavity dispersion-solvent-structure protocol for the nonelectrostatic contribution to the free energy of solvation. In some cases, the explicit solvent molecules are also added as reactant to the reaction system to stabilize the anions. Computed structures are illustrated using CYLView⁴¹. The H atom on α -C atom and the hydroxyl H atom of CH₃CH₂OH discussed in the paper, are marked with the superscript 'a' and 'b', respectively, namely CH₃CH^a₂OH or CH₃CH₂OH^b.

3 Results and Discussion

3.1 Validation of the Computational Method



Previous DFT studies⁴²⁻⁴⁶ were reported to investigate the radical reaction mechanism in organic pollutions degradation. It is shown that the B3LYP results are reasonably in agreement with the experimental observations. Specially, Cagnina et al.⁴⁷ investigated the decomposition mechanism of ammonium nitrite in the gas phase theoretically, and then a DFT benchmark was made with respect to CBS-QB3

reference value, which revealed that M06-2X functional provides a balanced description of thermodynamics and kinetics for the ammonium nitrite decomposition including the intermediate structures.

In order to select a suitable method, two typical reactions in our research system were selected to calculate with different computational methods, including B3LYP, M06-2X, MP2 and CCSD. As shown in eq 1 and 2, the first one is a hydrogen atom transfer reaction (eq 1), which is a key step in the carbonyl reduction process of this work. The second one is the debromination reduction process (eq 2) in this work.

3.1.1 Comparison in Geometries of the Transition State

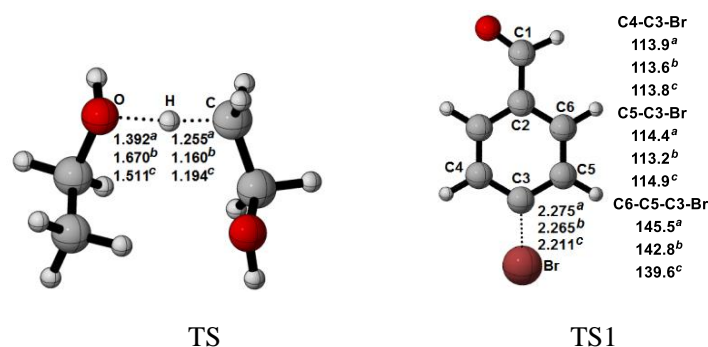


Fig. 1 The optimized geometries of the transition states (bond distances in angstroms, angles in degree) of the chosen reactions at B3LYP^a, M06-2X^b and MP2^c levels in ethanol solvent

The optimized geometries of the transition states for these two reactions are shown in Fig. 1. For the proton transfer reaction, M06-2X and MP2 structures are close to each other, the transfer hydrogen atom is close to the carbon atom. The differences between the O...H and C...H distances are 0.510 Å and 0.317 Å for M06-2X and MP2, respectively, while the difference is only 0.137 Å for B3LYP method, which indicates that the M06-2X results is closer to the MP2 results. The

similar conclusion can be get from the optimized geometry of the transition states of debromination reaction.

3.1.2 Comparison in Relative Energy

Table 1 The relative energies using different methods for eq 1 in ethanol solvent

		E (a.u.)	ΔE (a.u.)	ΔE (kcal/mol)
B3LYP	R	-309.918824	0.000000	0.0
	TS	-309.914048	0.004776	3.0
	P	-309.924601	-0.005777	-3.6
M06-2X	R	-309.747673	0.000000	0.0
	TS	-309.742522	0.005152	3.2
	P	-309.768704	-0.021031	-13.2
MP2	R	-308.927941	0.000000	0.0
	TS	-308.921617	0.006324	4.0
	P	-308.955253	-0.027311	-17.1
CCSD	R	-308.991832	0.000000	0.0
	TS	-308.985155	0.006677	4.2
	P	-309.023432	-0.031601	-19.8

Table 2 The relative energies using different methods for the process from IM1 to IM3 (eq 2) in ethanol solvent

		E (a.u.)	ΔE (a.u.)	ΔE (kcal/mol)
B3LYP	IM1	-2919.298992	0.000000	0.0
	TS1	-2919.289203	0.009789	6.1
	IM3+Br ⁻	-2919.292750	0.006241	3.9
M06-2X	IM1	-2919.179135	0.000000	0.0
	TS1	-2919.161461	0.017674	11.1
	IM3+Br ⁻	-2919.167484	0.011651	7.3
MP2	IM1	-2916.596741	0.000000	0.0
	TS1	-2916.585966	0.010775	6.8
	IM3+Br ⁻	-2916.588151	0.008590	5.4
CCSD	IM1	-2916.634851	0.000000	0.0
	TS1	-2916.621588	0.013263	8.3
	IM3+Br ⁻	-2916.623578	0.011273	7.1

The relative energies of these two chosen reactions for different methods are

shown in Table 1 and Table 2. The results show that for the hydrogen atom transfer reaction, both B3LYP and M06-2X methods perform very well for the reaction barrier, the relative energy difference is about 1 kcal/mol lower than that of the CCSD result. However, both DFT methods underestimate the heat of formation of this reaction, especially for the B3LYP method. Relative to the CCSD result, -19.8 kcal/mol, the heat of formation is only -3.6 kcal/mol for B3LYP. The result of M06-2X is -13.2 kcal/mol, which is much better than that of B3LYP. For the debromination reaction, B3LYP still underestimates the energy barrier of about 2.2 kcal/mol than that of CCSD result. However, M06-2X overestimates the energy barrier of about 2.8 kcal/mol. Relative to CCSD result, the difference in heat of formation is about 3.2 kcal/mol and 0.2 kcal/mol for B3LYP and M06-2X, respectively.

In conclusion, the M06-2X method offers a more reliable description of the reactions than B3LYP for the research system. Hence, taking the computational time and resource into account, the M06-2X method was applied in this work.

3.2 The Geometries of 4-BBA and IM1

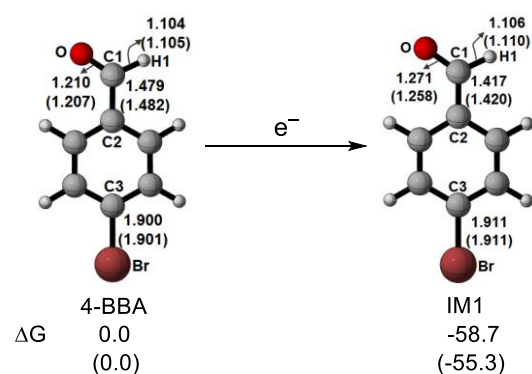
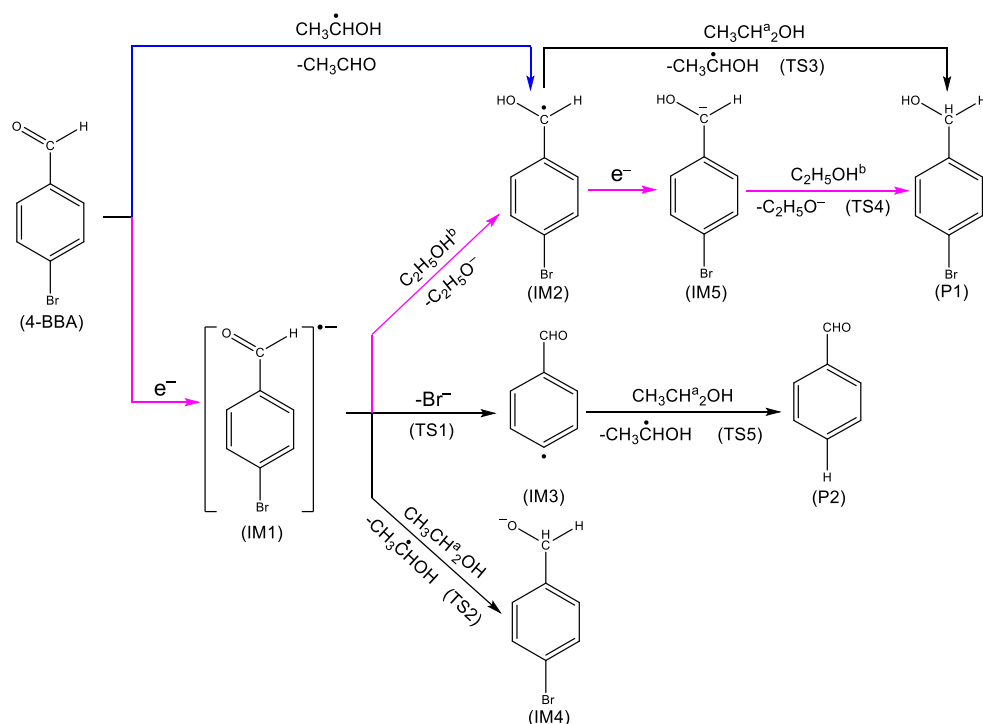


Fig. 2 The optimized geometries (bond lengths in angstroms) and relative free energies (kcal/mol) of 4-BBA and IM1 in ethanol (and in acetonitrile) solvent

In experiments, the photoelectron can be generated by the UV irradiation. Then 4-BBA can receive a photoelectron to form 4-BBA radical anion IM1. The optimized geometries and free energies of 4-BBA and IM1 are depicted in Fig. 2. In ethanol solvent, for the receiving photoelectron process (4-BBA→IM1), the C1-O distance is stretched to 1.271 Å from 1.210 Å, while the C1-C2 distance decreases to 1.417 Å from 1.479 Å. In acetonitrile solvent, for the transformation from 4-BBA to IM1, the C1-O distance is elongated to 1.258 Å from 1.207 Å, while the C1-C2 distance is shorten to 1.420 Å from 1.482 Å. In contrast, the distances of C1-H1 and C3-Br have a little alteration. Besides, the structures of 4-BBA and IM1 have no significant changes in different solvents, and the biggest difference is the C1-O distance (only 0.013 Å) for IM1. The results reveal that the effect of the solvents is similar in structure to each other for 4-BBA or IM1. Our calculations show that the exothermicities of this process are 58.7 kcal/mol and 55.3 kcal/mol in ethanol and acetonitrile solvents, respectively, as shown in Fig. 2.

3.3 Reaction Mechanism in Ethanol Solvent

Scheme 2 The proposed reaction mechanism for the process of 4-BBA being reduced to P1 and P2 in ethanol solvent photo-catalyzed by TiO₂ (The blue line and the pink line represent the dominant pathways)



The proposed reaction mechanism for the process of 4-BBA being reduced to 4-bromobenzyl alcohol (P1) and benzaldehyde (P2) in ethanol solvent photo-catalyzed by TiO_2 is shown in Scheme 2. It is divided into the two segments: the $\cdot\text{CH}(\text{OH})\text{CH}_3$ radical reduction process and the photoelectron reduction process.

In the $\cdot\text{CH}(\text{OH})\text{CH}_3$ radical reduction process, the hydroxyl H atom of $\cdot\text{CH}(\text{OH})\text{CH}_3$ radical could be abstracted by the O atom of 4-BBA with no free energy barrier, yielding a radical intermediate IM2 and CH_3CHO . In the photoelectron reduction process, 4-BBA can receive a photoelectron to form 4-BBA radical anion IM1 firstly. In the following process, starting from IM1, there are three possible different pathways to form IM2, IM3, and IM4, respectively (see Scheme 2).

Table 3 The relative Gibbs free energies during the reaction from IM1 to IM2 assisted by zero to five water molecules in ethanol solvent

	G (a.u.)	ΔG (a.u.)	ΔG (kcal/mol)
$\text{IM1} + \text{C}_2\text{H}_5\text{OH}^{\text{b}}$	-3074.064052	0.000000	0.0
$\text{IM2} + \text{C}_2\text{H}_5\text{O}^-$	-3074.039065	0.024987	15.7
$\text{IM1} + \text{C}_2\text{H}_5\text{OH}^{\text{b}} + 1\text{H}_2\text{O}$	-3150.471599	0.000000	0.0
$\text{IM2} + \text{C}_2\text{H}_5\text{O}^- + 1\text{H}_2\text{O}$	-3150.453637	0.017962	11.3

$\text{IM1}+\text{C}_2\text{H}_5\text{OH}^{\text{b}}+2\text{H}_2\text{O}$	-3226.879222	0.000000	0.0
$\text{IM2}+\text{C}_2\text{H}_5\text{O}^-+2\text{H}_2\text{O}$	-3226.863717	0.015505	9.7
$\text{IM1}+\text{C}_2\text{H}_5\text{OH}^{\text{b}}+3\text{H}_2\text{O}$	-3303.283425	0.000000	0.0
$\text{IM2}+\text{C}_2\text{H}_5\text{O}^-+3\text{H}_2\text{O}$	-3303.273588	0.009837	6.2
$\text{IM1}+\text{C}_2\text{H}_5\text{OH}^{\text{b}}+4\text{H}_2\text{O}$	-3379.691997	0.000000	0.0
$\text{IM2}+\text{C}_2\text{H}_5\text{O}^-+4\text{H}_2\text{O}$	-3379.684361	0.007636	4.8
$\text{IM1}+\text{C}_2\text{H}_5\text{OH}^{\text{b}}+5\text{H}_2\text{O}$	-3456.104052	0.000000	0.0
$\text{IM2}+\text{C}_2\text{H}_5\text{O}^-+5\text{H}_2\text{O}$	-3456.094675	0.009377	5.9

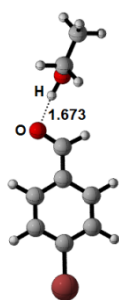
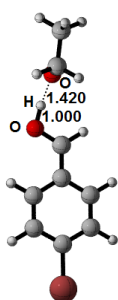
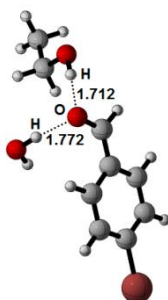
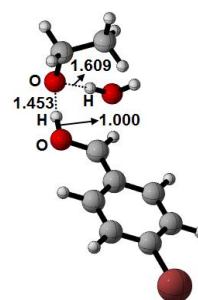
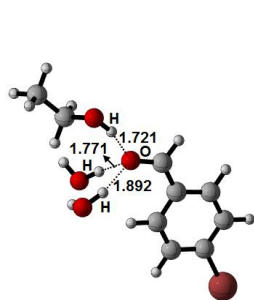
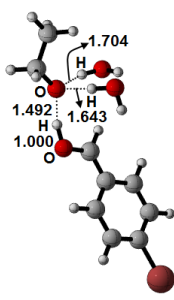
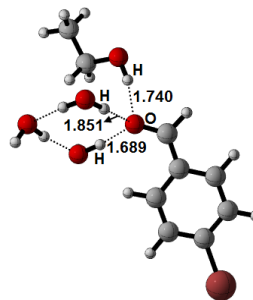
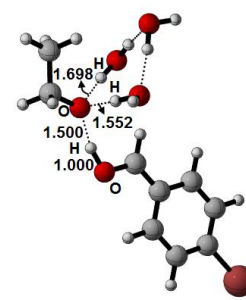
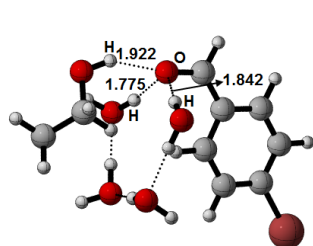
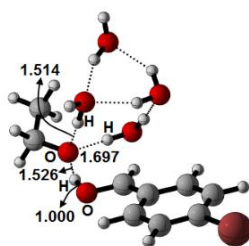
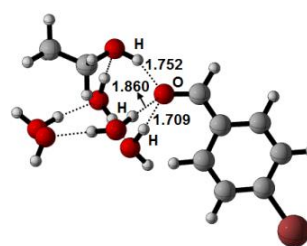
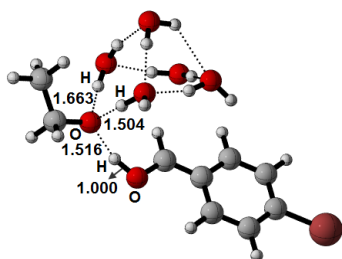
 $\text{IM1}+\text{C}_2\text{H}_5\text{OH}^{\text{b}}$  $\text{IM2}+\text{C}_2\text{H}_5\text{O}^-$  $\text{IM1}+\text{C}_2\text{H}_5\text{OH}^{\text{b}}+1\text{H}_2\text{O}$  $\text{IM2}+\text{C}_2\text{H}_5\text{O}^-+1\text{H}_2\text{O}$  $\text{IM1}+\text{C}_2\text{H}_5\text{OH}^{\text{b}}+2\text{H}_2\text{O}$  $\text{IM2}+\text{C}_2\text{H}_5\text{O}^-+2\text{H}_2\text{O}$  $\text{IM1}+\text{C}_2\text{H}_5\text{OH}^{\text{b}}+3\text{H}_2\text{O}$  $\text{IM2}+\text{C}_2\text{H}_5\text{O}^-+3\text{H}_2\text{O}$  $\text{IM1}+\text{C}_2\text{H}_5\text{OH}^{\text{b}}+4\text{H}_2\text{O}$  $\text{IM2}+\text{C}_2\text{H}_5\text{O}^-+4\text{H}_2\text{O}$  $\text{IM1}+\text{C}_2\text{H}_5\text{OH}^{\text{b}}+5\text{H}_2\text{O}$ 



Fig. 3 The optimized geometries (bond distances in angstroms, angles in degree) of the reactants and products in the process from IM1 to IM2 assisted by zero to five water molecules in ethanol solvent

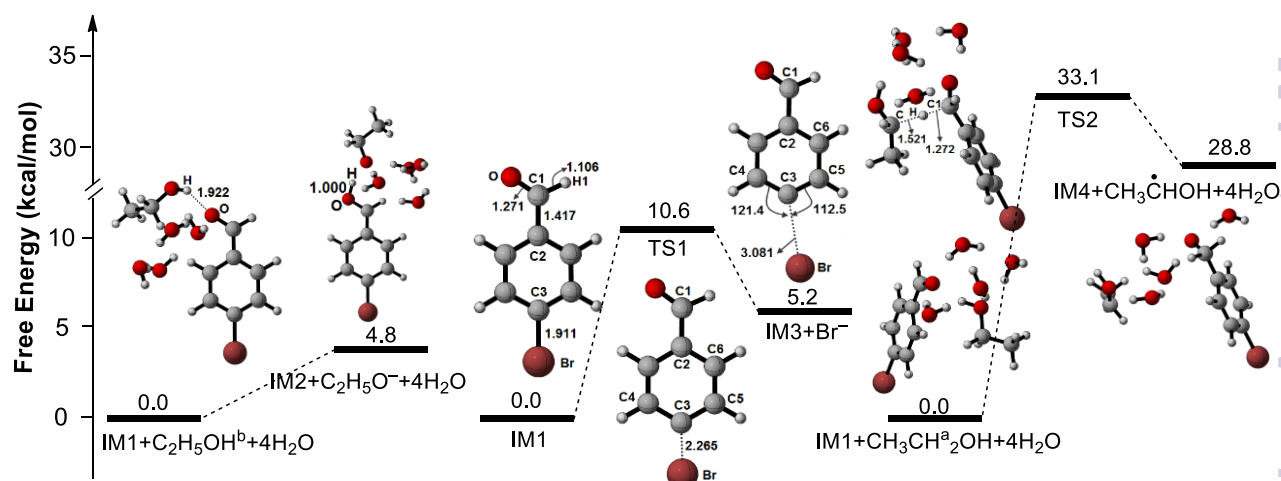


Fig. 4 The Gibbs free energy profile (kcal/mol) for the processes from IM1 to IM2, IM3 and IM4 in ethanol solvent, respectively, replete with the optimized structures (bond distances in angstroms, angles in degree)

Interestingly, in the process of forming IM2, all attempts to optimize the complex of the product $\text{IM2} + \text{C}_2\text{H}_5\text{O}^-$ were failed because it went back to the reactant $\text{IM1} + \text{C}_2\text{H}_5\text{OH}^b$, which might indicate that the $\text{C}_2\text{H}_5\text{O}^-$ is unstable without the stabilization of the solvent molecule. However, according to the study of Dmitenko et al.'s⁴⁸, the explicit solvent molecules played a very important role in the ion stabilization and dropping the endothermicity of the reaction. In Pruden et al.'s³ experiment, the 95% ethanol was used. Thus, there are water molecules in the reaction system, which may stabilize the anions during the reaction. Taking this effect into account, several water molecules (the number is from zero to five) were added to stabilize the $\text{C}_2\text{H}_5\text{O}^-$ anion or the O^- of IM1 through the hydrogen bonds (see Fig. 3). With the distance between H atom and O atom of the IM2 being fixed to 1.000 Å⁴⁸⁻⁵⁰, as displayed in Fig. 3, the relative Gibbs free energies are calculated. As expected, the endothermicity decreases gradually from 15.7 kcal/mol to 4.8 kcal/mol

with the water molecules numbers increasing from zero to four (see Table 3), whereas the endothermicity slightly increases with the water molecules numbers increasing to five, which indicates that the $\text{C}_2\text{H}_5\text{O}^-$ anion can be well stabilized by water molecules. In consideration of the large difference in concentration between the $\text{C}_2\text{H}_5\text{O}^-$ and the $\text{C}_2\text{H}_5\text{OH}$, from the viewpoint of chemical equilibrium, in ethanol solvent, the hydroxyl H atom of the $\text{C}_2\text{H}_5\text{OH}^b$ may be abstracted by IM1 with the anion stabilized by four water molecules, producing an intermediate IM2 and $\text{C}_2\text{H}_5\text{O}^-$. In addition, the corresponding Gibbs free energy profiles in ethanol solvent is provided in Fig. 4, replete with the optimized geometries of the reactants, intermediates, transition structures, and products.

The formation mechanism of the IM3 is a debromination process through a transition state TS1. In ethanol solvent, for the debromination process (IM1 \rightarrow IM3), the C3-Br distance is elongated to 2.265 Å in TS1 from 1.911 Å in IM1, subsequently relaxing to an intermediate IM3 and Br^- . It is noted that the C6-C5-C3-Br dihedral angle in TS1 is 142.9°, while it becomes to 165.6° in IM3+ Br^- . Additionally, the angles of C4-C3-Br and C5-C3-Br are 121.4° and 112.5° in ethanol solvent, respectively. The phenomenon is attributed to the Coulombic repulsion between the single occupied orbital on C3 atom of the IM3 and the bromide anion.

Regarding to the process of forming IM4, with the anion stabilized by four water molecules, the H atom on α -C atom of the $\text{CH}_3\text{CH}^a_2\text{OH}$ could be abstracted by IM1 through a transition state TS2, with the distances of $\text{C}\cdots\text{H}$ and $\text{C1}\cdots\text{H}$ being 1.521 Å and 1.272 Å, respectively, producing IM4 and the $\cdot\text{CH}(\text{OH})\text{CH}_3$ radical.

As shown in Fig. 4, in ethanol solvent, the transformation from IM1 to IM2 proceeds easily with no free energy barrier with the anion stabilized by four water molecules, and it is endothermic by 4.8 kcal/mol. In contrast, the debromination process (IM1 \rightarrow IM3) involves a free energy barrier of 10.6 kcal/mol and an endothermicity of 5.2 kcal/mol. The process of converting IM1 to IM4 is disfavored either in kinetics or thermodynamics, as the free energy barrier is as high as 33.1 kcal/mol and it is endothermic by 28.8 kcal/mol. Hence, it is more favored to form IM2 from IM1 in thermodynamics; *i.e.*, the reaction may occur along the pathway of

forming IM2.

Table 4 The calculated Gibbs free energies of 4-BBA, IM1, IM2, and IM5 in ethanol solvent

	G (a.u.)	ΔG (a.u.)	ΔG (kcal/mol)
4-BBA	-2919.022117		
IM1	-2919.115612	-0.093495	-58.7
IM2	-2919.574662		
IM5	-2919.673551	-0.098889	-62.1

It's interesting to know which one is the better electron acceptor when they are in the same condition, the 4-BBA molecule, or the IM2 radical. As show in Table 4, the calculation results predict that the IM2 radical is the better one, since it releases 3.4 kcal/mol heat when accepting an electron. These results indicate that the two electron process is possible in thermodynamics.

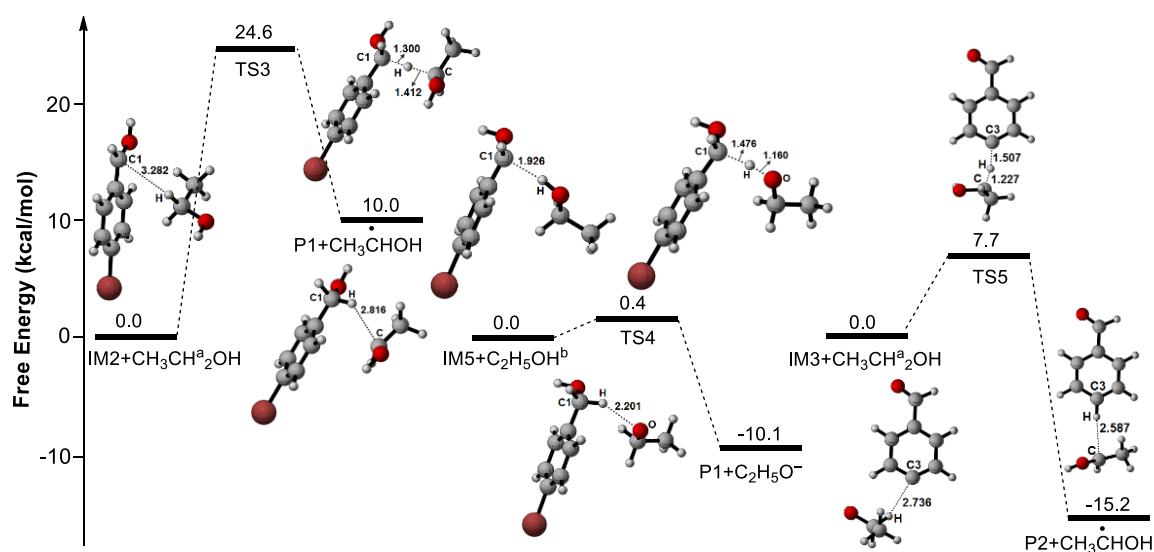


Fig. 5 The Gibbs free energy profile (kcal/mol) for the processes from IM2, IM3, and IM5 to P1 and P2 in ethanol solvent, respectively, replete with the optimized structures (bond distances in angstroms, angles in degree)

In the following steps, there are two possible pathways to form P1 and one pathway to form P2, as show in Scheme 2. Besides, the corresponding Gibbs free energy profile for the processes from IM2, IM3, and IM5 to P1 and P2 in ethanol

solvent is given in Fig. 5.

One possible pathway for IM2 to P1 is as follow: the H atom on α -C atom of the $\text{CH}_3\text{CH}^{\text{a}}_2\text{OH}$ could be abstracted by IM2, experiencing a transition state TS3. The $\text{C1}\cdots\text{H}$ distance decreases to 1.300 Å (TS3) from 3.282 Å ($\text{IM2}+\text{CH}_3\text{CH}^{\text{a}}_2\text{OH}$), while the $\text{C}\cdots\text{H}$ distance increases to 2.816 Å ($\text{P1}+\bullet\text{CH}(\text{OH})\text{CH}_3$) from 1.412 Å (TS3), producing P1 and the $\bullet\text{CH}(\text{OH})\text{CH}_3$ radical. In the other pathway, as proposed by Purden et al.³, IM2 can receive a photoelectron to form IM5, subsequently IM5 abstracts the hydroxyl H atom of the $\text{C}_2\text{H}_5\text{OH}^{\text{b}}$ via a transition state TS4. In this process, the $\text{C1}\cdots\text{H}$ distance is shorten to 1.476 Å (TS4) from 1.926 Å ($\text{IM5}+\text{C}_2\text{H}_5\text{OH}^{\text{b}}$), the $\text{C}\cdots\text{H}$ distance is elongated to 2.201 Å ($\text{P1}+\text{C}_2\text{H}_5\text{O}^-$) from 1.160 Å (TS4), to yield the carbonyl reduction product P1 and $\text{C}_2\text{H}_5\text{O}^-$.

For the process of converting IM3 to P2, the H atom on α -C atom of the $\text{CH}_3\text{CH}^{\text{a}}_2\text{OH}$ is abstracted by the $\bullet\text{C3}$ radical of IM3 through a transition state TS5. In TS5, the $\text{C3}\cdots\text{H}$ distance decreases to 1.507 Å from 2.736 Å ($\text{IM3}+\text{CH}_3\text{CH}^{\text{a}}_2\text{OH}$), whereas the $\text{C}\cdots\text{H}$ distance increases to 2.587 Å ($\text{P2}+\bullet\text{CH}(\text{OH})\text{CH}_3$) from 1.227 Å. Successively, the formation of C3-H bond yields the debromination product P2.

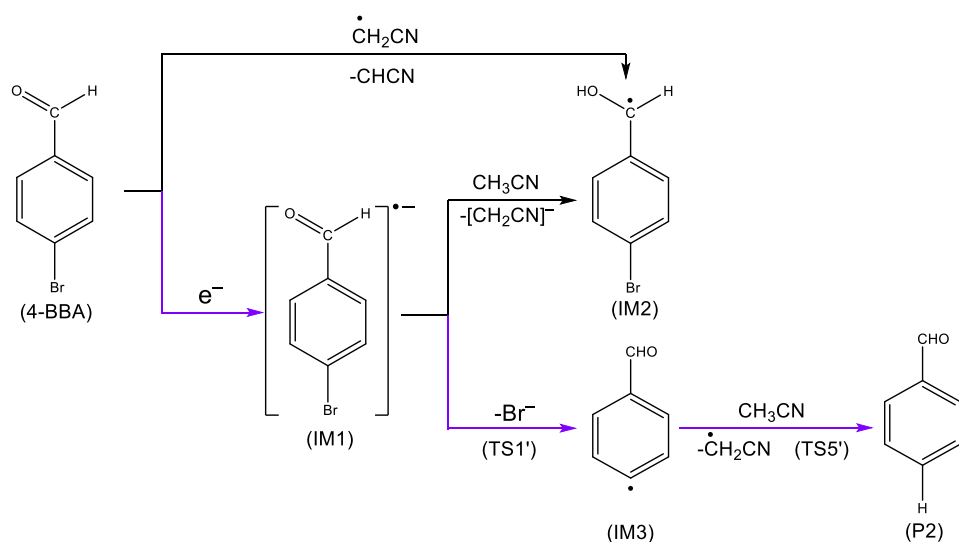
As show in Fig. 5, our results reveal that the transformation from the $\text{IM2}+\text{CH}_3\text{CH}^{\text{a}}_2\text{OH}$ to the $\text{P1}+\bullet\text{CH}(\text{OH})\text{CH}_3$ is disfavored either in kinetics or in thermodynamics, since the free energy barrier is as high as 24.6 kcal/mol and it is endothermic by 10.0 kcal/mol. However, for the process from IM5 to P1, it involves only the very low free energy barrier of 0.4 kcal/mol and the exothermicity of 10.1 kcal/mol, indicating that this reaction proceeds easily both in kinetics and in thermodynamics. In the process from IM3 to P2, the free energy barrier is calculated to be 7.7 kcal/mol, and it is exothermic by 15.2 kcal/mol. Considered that the forward step of the debromination process is endothermic by 5.2 kcal/mol, the total thermodynamic effect of this process is exothermic by 10.0 kcal/mol. Thus, in ethanol solvent, the process of forming P1 is more favorable through the pathway from IM5 in kinetics.

In a word, in ethanol solvent, the 4-BBA could be reduced to the 4-bromobenzyl alcohol through a two-step process of the electron transfer or the alcohol radical

reduction pathway, but not the reduction product of debromination.

3.4 Reaction Mechanism in Acetonitrile Solvent

Scheme 3 The proposed reaction mechanism for the process of the 4-BBA being reduced to P2 in acetonitrile solvent photo-catalyzed by TiO₂ (The purple line represents the dominant pathway)



The proposed reaction pathway for the process of the 4-BBA being reduced to P2 is provided in Scheme 3. It consists of the two segments: the hydrogen abstraction process from $\bullet\text{CH}_2\text{CN}$ and the receiving electron process.

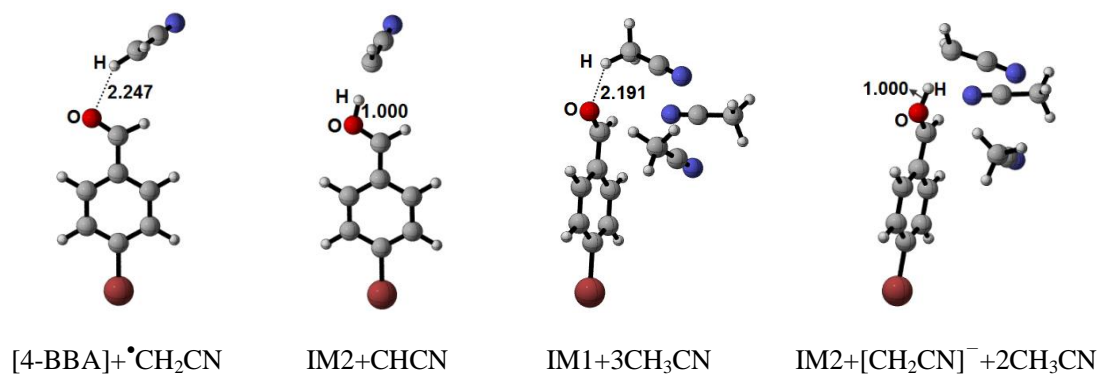


Fig. 6 The optimized geometries (bond distances in angstroms, angles in degree) of the reactants and products in the processes from 4-BBA or IM1 to IM2 in acetonitrile solvent

In the hydrogen abstraction process from $\bullet\text{CH}_2\text{CN}$, the O \cdots H distance of

[4-BBA]+•CH₂CN is predicted to be 2.247 Å (see Fig. 6), while the stable structure of IM2+CHCN is not obtained. To estimate the free energy for this process, the distance between H atom and O atom of IM2 in the IM2+CHCN is fixed to 1.000 Å (see Fig. 6) during the calculations⁴⁸⁻⁵⁰. As shown in Table 5, the calculated free energy of product (IM2+CHCN) is 46.1 kcal/mol higher than that of reactant ([4-BBA]+•CH₂CN), revealing that this reaction is difficult to take place in acetonitrile solvent.

Regarding to the pathway from IM1 to IM2, with the stabilization of the two CH₃CN molecules, the O...H distance of IM1+3CH₃CN is calculated to be 2.191 Å (see Fig. 6), while all attempts to optimize the structure of the IM2+[CH₂CN]⁻ are not successful. To obtain this structure, a geometry optimization is performed in which the O-H distance between H atom and O atom of IM2 in the IM2+[CH₂CN]⁻+2CH₃CN is fixed to 1.000 Å (see Fig. 6) during the optimization process⁴⁸⁻⁵⁰. The free energy for the structure of (IM2+[CH₂CN]⁻+2CH₃CN) is 20.7 kcal/mol higher than that of reactant (IM1+3CH₃CN), as summarized in Table 5, indicating that in acetonitrile solvent this reaction is disfavored in thermodynamics.

Table 5 The relative Gibbs free energies during the reaction from 4-BBA to IM2 in acetonitrile solvent

	G (a.u.)	ΔG (a.u.)	ΔG (kcal/mol)
[4-BBA]+•CH ₂ CN	-3051.077294	0.000000	0.0
IM2+CHCN	-3051.003776	0.073518	46.1
IM1+3CH ₃ CN	-3317.229180	0.000000	0.0
IM2+[CH ₂ CN] ⁻ +2CH ₃ CN	-3317.196204	0.032976	20.7

The Gibbs free energy profile for the process of 4-BBA being reduced to P2 in acetonitrile solvent is shown in Fig. 7, replete with the optimized structures. The debromination reaction is a two-step reaction: the elimination of bromide anion, and the hydrogen abstraction reaction from solvent molecule CH₃CN.

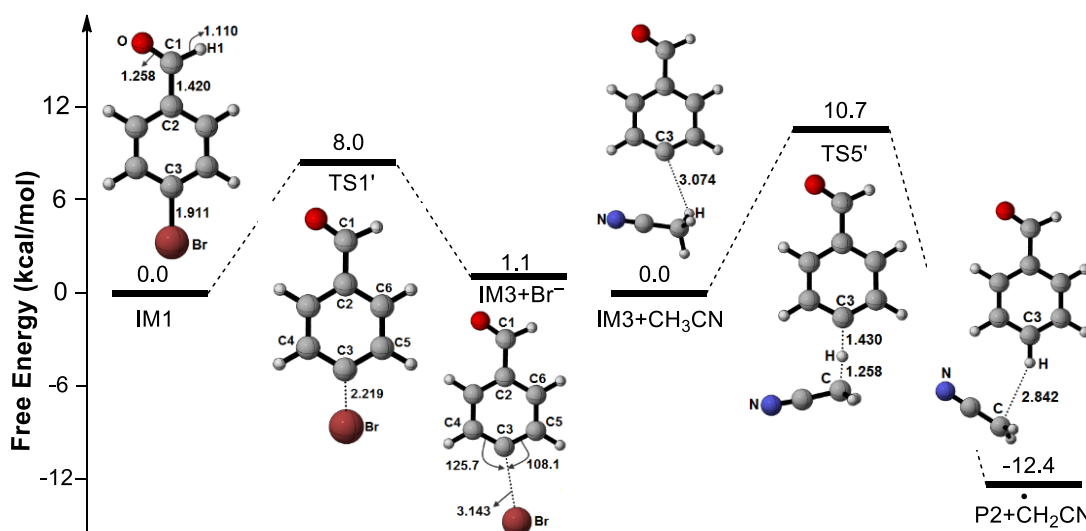


Fig. 7 The Gibbs free energy profile (kcal/mol) for the process of 4-BBA being reduced to P2 in acetonitrile solvent, replete with the optimized structures (bond distances in angstroms, angles in degree)

The first step of the mechanism is the elimination of bromide anion process through a transition state TS1'. In acetonitrile solvent, for the debromination process (IM1→IM3), the C3-Br distance is elongated to 2.219 Å in TS1' from 1.911 Å in IM1, subsequently relaxing to an intermediate IM3 and Br⁻. It is noticeable that the dihedral angle of the C6-C5-C3-Br in the TS1' is 143.4°, and it becomes to 166.2° in the IM3+Br⁻. Additionally, the angles of C4-C3-Br and C5-C3-Br are respectively 125.7° and 108.1° in acetonitrile solvent. The same phenomenon also appears in ethanol solvent, and it is attributed to the Coulombic repulsion between the single occupied orbital on C3 atom of the IM3 and the bromide anion. This step should proceed easily in kinetics, with the free energy barrier of 8.0 kcal/mol.

This is followed by the hydrogen abstraction reaction from solvent molecule. In acetonitrile solvent, the methyl H atom of the CH₃CN could be abstracted by IM3 via a transition state TS5', with the distance of C3...H decreasing to 1.430 Å (TS5') from 3.074 Å (IM3+CH₃CN), subsequently the distance of C...H between methyl C atom and H atom of CH₃CN increasing to 2.842 Å (P2+•CH₂CN) from 1.258 Å (TS5'), finally releasing the debromination product P2 and the •CH₂CN radical. This is the rate-determining step in this reaction, with a low free energy barrier of 10.7 kcal/mol.

Moreover, the IM3→P2 step is exothermic by 12.4 kcal/mol. This implies that in acetonitrile solvent, the process of forming P2 is favored both in thermodynamics and in kinetics.

In summary, our calculated results show that in acetonitrile solvent, the 4-BBA could be reduced to benzaldehyde via the debromination reduction, not the 4-bromobenzyl alcohol.

4 Conclusions

We have studied the selective photoreduction mechanism of the 4-BBA on TiO₂ in ethanol and acetonitrile solvents by employing DFT calculations at the M06-2X/6-311G* level. The following conclusions have been reached:

(1) The 4-BBA could be reduced to 4-bromobenzyl alcohol in ethanol solvent, while it is reduced to benzaldehyde in acetonitrile solvent, which is consistent with the experiment observation.

(2) In ethanol solvent, the calculation results predict that the carbonyl reduction occurs through two competitive two-step processes, a two electron reduction steps or an alcohol radical reduction followed by an electron reduction step. Our calculation results support that the alcohol radical reduction may play an important role in the photoreduction process.

(3) In the carbonyl reduction process, the proton abstracting reaction from the CH₃CH₂OH is selective. The calculation results predict that in the electron reduction step, the anion intermediate abstracts the proton in hydroxyl of CH₃CH₂OH, but not the α proton of CH₃CH₂OH; While in the alcohol radicals reduction step, the reactant abstracts the hydrogen atom from hydroxyl of \bullet CH(OH)CH₃ radical. The results are in accordance with the O-deuterated ethanol (C₂H₅OD) experiment.

Acknowledgement

Financial support is grateful to the Project Supported by Guangdong Province Universities and Colleges Pearl River Scholar Funded Scheme, as well as the National

Natural Science Foundation of China (Nos. 21273081 and 21403074). The support from the Guangdong provincial department of science and technology is also greatly acknowledged.

References

- 1 C. Kotal, *J. Chem. Edu.*, 1983, **60**, 882-887.
- 2 K. Kalyansundaram and M. Grätzl, *Photochem. Photobiol.*, 1984, **40**, 807-821.
- 3 C. Joyce-Pruden, J. K. Pross and Y. Li, *J. Org. Chem.*, 1992, **57**, 5087-5091.
- 4 T. Zhang, L. You and Y. Zhang, *Dyes Pigments*, 2006, **68**, 95-100.
- 5 F. Mahdavi, T. C. Bruton and Y. Li, *J. Org. Chem.*, 1993, **58**, 744-746.
- 6 S. O. Flores, O. Rios-Bernij, M. A. Valenzuela, I. Córdova, R. Gómez and R. Gutiérrez, *Top. Catal.*, 2007, **44**, 507-511.
- 7 K. Imamura, S. Iwasaki, T. Maeda, K. Hashimoto, B. Ohtani and H. Kominami, *Phys. Chem. Chem. Phys.*, 2011, **13**, 5114-5119.
- 8 P. Eskandari, F. Kazemi and Z. Zand, *J. Photoch. Photobio. A*, 2014, **274**, 7-12.
- 9 Z. Zand, F. Kazemi and S. Hosseini, *Tetrahedron Lett.*, 2014, **55**, 338-341.
- 10 S. Yanagida, Y. Ishimaru, Y. Miyake, T. Shiragami and C. Pac, *J. Phys. Chem.*, 1989, **93**, 2516-2582
- 11 S. Kohmoto, T. Kreher, M. Yamamoto and K. Yamada, *Bull. Chem. Soc. Jpn.*, 1990, **63**, 3689-3700.
- 12 K. Tsunashima and T. Nonaka, *Electrochim. Acta*, 1997, **42**, 2081-2087.
- 13 J. W. Park, E. K. Kim and K. K. Park, *Bull. Korean Chem. Soc.*, 2002, **23**,

- 1229-1234.
- 14 S. Kohtani, E. Yoshioka, K. Saito, A. Kudo and H. Miyabe, *J. Phys. Chem. C.*, 2012, **116**, 17705-17713.
- 15 E. A. Escobar, M. Á. V. Zapata, S. A. Hernández, S. O. F. Valle, O. R. Berny, V. J. G. Ángeles and I. C. Reyes, *J. Mex. Chem. Soc.*, 2010, **54**, 133-138.
- 16 R. L. Calhoun, K. Winkelmann and G. Mills, *J. Phys. Chem. B*, 2001, **105**, 9739-9746.
- 17 J. L. Ferry and W. H. Glaze, *Langmuir*, 1998, **14**, 3551-3555.
- 18 W. Wu, L. Wen, L. Shen, R. Liang, R. Yuan and L. Wu, *Appl. Catal. B: Environ.*, 2013, **130-131**, 163-167.
- 19 M. Puchala, *Radiat. Environ. Biophys.*, 1994, **33**, 325-339.
- 20 Y. Yin, X. Xu, X. Ge and Z. Zhang, *Radiat. Phys. Chem.*, 1998, **53**, 567-570.
- 21 V. N. H. Nguyen, R. Amal and D. Beydoun, *Chem. Eng. Sci.*, 2003, **58**, 4429-4439.
- 22 H. He, P. Zapol and L. A. Curtiss, *Energy Environ. Sci.*, 2012, **5**, 6196-6205.
- 23 D. Lee and Y. Kanai, *J. Am. Chem. Soc.*, 2012, **134**, 20266-20269.
- 24 G. Rotko, P. P. Romańczyk, G. Andryianau, S. S. Kurek, *Electrochem. Commun.*, 2014, **43**, 117-120.
- 25 X. Huang, L. Peng, S. Li and F. L. Gu, *Theor. Chem. Acc.*, 2015, **134**, 1-12.
- 26 M. J. Frisch, G. W. Trucks, H. B. Schlegel, G. E. Scuseria, M. A. Robb, J. R. Cheeseman, G. Scalmani, V. Barone, B. Mennucci, G. A. Petersson, H. Nakatsuji, M. Caricato, X. Li, H. P. Hratchian, I. A. F., J. Bliino, G. Zheng, J. L. Sonnenberg, M. Hada, K. T. Ehara, R. Fukuda, J. Hasegawa, M. Ishida, N. T.,

- H. O. K. Y., H. Nakai, T. Vreven, J. A. Montgomery, Jr., J. E. Peralta, F. Ollari, M. Bearpark, J. J. Heyd, E. Brothers, K. N. Kudin, V. N. Straroverov, T. Keith, R. Kobayashi, J. Normand, K. R. Raghavachari, A. Jendell, J. C. Burant, S. S. Iyengar, J. Tomasi, M. Cossi, J. M. Millam, M. Klene, J. E. Knox, J. B. Cross, V. Bakken, C. Adamo, J. Jaramillo, R. Gomperts, R. E. Stratmann, O. Yazyev, A. J. Austin, R. Cammi, C. Pomelli, J. W. Ochterski, R. L. Martin, K. Morokuma, V. G. Zakrzewski, G. A. Voth, P. Salvador, J. J. Dannenberg, S. Dapprich, A. D. Daniels, O. Farkas, J. B. Foresman, J. V. Ortiz, J. Cioslowski and D. J. Fox, *Gaussian 09*, Gaussian Inc., Wallingford CT, 2010.
- 27 Y. Zhao and D. G. Truhlar, *Theor. Chem. Acc.*, 2008, **120**, 215-241.
- 28 A. D. Becke, *J. Chem. Phys.*, 1993, **98**, 5648-5652.
- 29 C. Lee, W. Yang and R. G. Parr, *Phys. Rev. B*, 1988, **37**, 785-789.
- 30 B. Miehlich, A. Savin, H. Stoll and H. Preuss, *Chem. Phys. Lett.*, 1989, **157**, 200-206.
- 31 M. Head-Gordon and J. A. Pople, *Chem. Phys. Lett.*, 1988, **153**, 503-506.
- 32 S. Saebø and J. Almlöf, *Chem. Phys. Lett.*, 1989, **154**, 83-89.
- 33 M. J. Frisch, *Chem. Phys. Lett.*, 1990, **166**, 275-280.
- 34 M. J. Frisch, *Chem. Phys. Lett.*, 1990, **166**, 281-289.
- 35 M. Head-Gordon and T. Head-Gordon, *Chem. Phys. Lett.*, 1994, **220**, 122-128.
- 36 G. D. Purvis and R. J. Bartlett, *J. Chem. Phys.*, 1982, **76**, 1910-1918.
- 37 G. E. Scuseria, C. L. Janssen and H. F. Schaefer, *J. Chem. Phys.*, 1988, **89**, 7382-7387.
- 38 G. E. Scuseria and H. F. Schaefer, *J. Chem. Phys.*, 1989, **90**, 3700-3703.
- 39 K. Fukui, *Acc. Chem. Res.*, 1981, **14**, 363-368.

- 40 A. V. Marenich, C. J. Cramer and D. G. Truhlar, *J. Phys. Chem. B*, 2009, **113**, 6378-6396.
- 41 C. Y. Legault, CYLView, version 1.0b, Université de Sherbrooke: Sherbrooke, Quebec, Canada, 2009.
- 42 A. R. Nicolaescu, O. Wiest and P. V. Kamat, *J. Phys. Chem. A*, 2005, 109, 2829-2835.
- 43 A. Hatipoglu, D. Vione, Y. Yalçın, C. Minero and Z. Çınar, *J. Photoch. Photobio. A*, 2010, 215, 59-68.
- 44 M. Kılıç, G. Koçtürk, N. San and Z. Çınar, *Chemosphere*, 2007, 69, 1396-1408.
- 45 Z. Han, D. Zhang, Y. Sun and C. Liu, *Chem. Phys. Lett.*, 2009, 474, 62-66.
- 46 L. Wang and A. Tang, *Chemosphere*, 2012, 89, 950-956.
- 47 S. Cagnina, P. Rotureau, G. Fayet and C. Adamo, *Phys. Chem. Chem. Phys.*, 2013, 15, 10849-10858.
- 48 O. Dmitrenko, C. Thorpe and R. D. Bach, *J. Org. Chem.*, 2007, **72**, 8298-8307.
- 49 N. Lehnert, V. K. K. Praneeth and F. Paulat, *J. Comput. Chem.*, 2006, **27**, 1338-1351.
- 50 M. Boronat, P. Viruela and A. Corma, *J. Phys. Chem. B*, 1997, **101**, 10069-10074.